Avoiding a Spanning Cluster in Percolation Models

Y. S. Cho *et al.*

Science **339**, 1185 (2013);
DOI: 10.1126/science.1230813

Science (print ISSN 0036-8075; online ISSN 1095-9203) is published weekly, except the last week in December, by the American Association for the Advancement of Science, 1200 New York Avenue NW, Washington, DC 20005.

Avoiding a Spanning Cluster in Percolation Models

Y. S. Cho,[1] S. Hwang,[1] H. J. Herrmann,[2] B. Kahng[1]*

When dynamics in a system proceeds under suppressive external bias, the system can undergo an abrupt phase transition, as can happen when an epidemic spreads. Recently, an explosive percolation (EP) model was introduced to understand such phenomena. The order of the EP transition has not been clarified in a unified framework covering low-dimensional systems and the mean-field limit. We introduce a stochastic model in which a rule for dynamics is designed to avoid the formation of a spanning cluster through competitive selection in Euclidean space. We use heuristic arguments to show that in the thermodynamic limit and depending on a control parameter, the EP transition can be either continuous or discontinuous if $d < d_c$ and is always continuous if $d \geq d_c$, where d is the spatial dimension and d_c is the upper critical dimension.

The notion of percolation transition (PT) (*1*) is widely applied in a variety of disciplines; it explains the formation of a spanning cluster connecting two opposite sides of a system in Euclidean space, such as occurs in metal-insulator or sol-gel transitions. Alternatively, percolation can also be interpreted as the formation of a macroscopic cluster in the system, and this concept has been used to model the spread of epidemics (*2*) and the formation of opinions within social networks (*3*). These two pictures may be regarded as the same, but they can lead to different evolution processes in Euclidean space. Here, we study an abrupt PT (*4*) from these two perspectives.

One of the models in the more general second category is the classic Erdős and Rényi (ER) (*5*) model, in which the evolution proceeds as follows: Starting with N isolated nodes, an edge is connected between a randomly selected unconnected pair of nodes at each time step. Then, as the number of connected edges is increased, a macroscopic cluster is generated at the percolation threshold, and its size is increased continuously. Recently, the ER model was modified by imposing additionally a so-called product rule or sum rule, which suppresses the formation of a large cluster (*4*). Because of this suppressive bias, the percolation threshold is delayed; thus, when the giant cluster eventually emerges, it does so explosively. Hence, this model has been called the explosive percolation (EP) model. This result has attracted much interest (*6*–*23*), including openings toward other subjects such as synchronization phenomena (*23*), jamming in the Internet (*24*), and analysis of real-world networks (*25*). Initially, this explosive PT was regarded as a discontinuous transition; however, it was recently found that the transition is continuous in the thermodynamic limit (*9*), followed by a mathematical proof (*10*) and extensive supporting simulations (*11*–*13*). The random graph in fact represents the mean-field description of the model on a Euclidean lattice. EP problems in Euclidean space have also been considered, and the numerical results suggest discontinuous percolations (*14*). Because of the absence of analytic results, the order of explosive PT in Euclidean space has not yet been determined. Under this circumstance, it is of interest to clarify the order of the explosive PT in Euclidean space and on random graphs in a unified manner.

The product rule or sum rule was inspired by an idea first mathematically developed in (*26*, *27*) to investigate the power of multiple choices in random processes. These ideas were refined to what is called an Achlioptas process, in which one chooses the best among randomly given multiple options to avoid the formation of a certain target pattern (*28*). Here, we choose the spanning cluster rather than the giant cluster as the target pattern of the PT in Euclidean space. Surprisingly, this choice, while keeping the strategy of choosing the best among several options, enables us to determine analytically the order of the explosive PT for the spanning cluster in the thermodynamic limit. In this spanning cluster–avoiding (SCA) model, the transition can be either discontinuous or continuous below the upper critical dimension, depending on the number of potential bonds m introduced in the dynamic rule, and it is continuous above the upper critical dimension (i.e., in the mean-field limit). Thus, the appearance of an abrupt PT can be clarified within a unified scheme. Moreover, the analytic results and the methodology used in the SCA model can serve as a platform for understanding the PTs for other models showing abrupt transitions, such as the product rule (*4*) and the Gaussian model (*18*). In fact, the general mechanism underneath the abrupt PT is that by throttling spanning, the finite clusters can become very dense, so that when they finally merge to a percolating configuration, a substantial fraction of sites is immediately involved in the largest cluster.

We begin by introducing an adequate suppressing rule in Euclidean space. Starting with a d-dimensional regular square lattice of linear size L having $N = L^d$ nodes and $N_b = zN$ unoccupied bonds, where z is the coordination number divided by 2, we randomly choose at each time step m unoccupied bonds. They are classified into two types: bridge and nonbridge bonds. Bridge bonds are those that would form a spanning cluster if occupied. We want to avoid bridge bonds being occupied, and thus one of the nonbridge bonds is randomly selected and occupied (Fig. 1A). If the m potential bonds are all bridge bonds, then one of them is selected randomly and occupied (Fig. 1B). Once a spanning cluster is created, no more restrictions are imposed on the occupation of bonds. This procedure continues until all bonds are occupied. The selection rule among multiple options is inspired by the best-of-m model (*19*). We denote the number and the fraction of occupied bonds as ℓ and $t = \ell/zN$, respectively. By analogy to ordinary percolation, t can be interpreted as an occupation probability, and also as

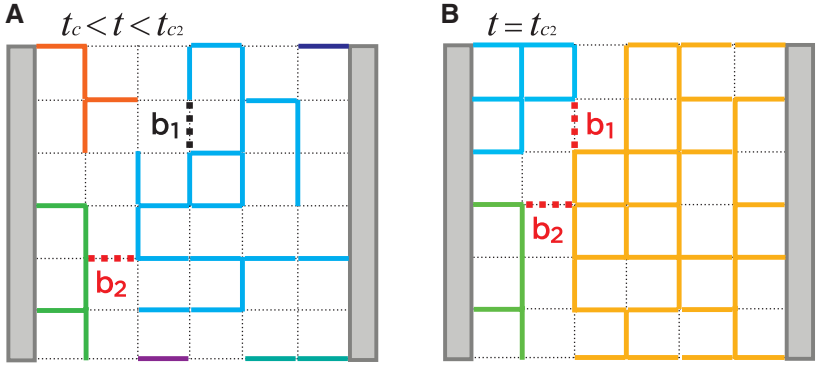

Fig. 1. (**A**) Dynamics of the SCA model on a square lattice. For the case $m = 2$, two empty bonds, b_1 and b_2 (shown as dashed lines), are randomly selected. If one of them is a bridge bond (b_2), by which a spanning cluster would be formed, then the nonbridge bond (b_1) is chosen. (**B**) At $t = t_{c2}$, two bridge bonds can be selected for the first time. Then, one of them is taken randomly and a spanning cluster is formed.

[1]Department of Physics and Astronomy, Seoul National University, Seoul 151-747, Korea. [2]Computational Physics for Engineering Materials, Institute for Building Materials, ETH Zürich, 8093 Zürich, Switzerland.

*To whom correspondence should be addressed. E-mail: bkahng@snu.ac.kr

the time of our dynamic system. We define ℓ_{cm} as the number of occupied bonds when a bridge bond is occupied for the first time. The percolation threshold is $t_{cm} \equiv \ell_{cm}/N_b$, which for $m > 1$ is larger than the percolation threshold t_c of ordinary percolation.

We performed extensive numerical simulations for various system sizes L and parameter values m to see (i) how the order parameter $G_m(t)$—the fraction of sites (nodes) belonging to the spanning cluster—behaves as a function of t and m, and (ii) how the percolation threshold t_{cm} averaged over configurations depends on m, L, and dimension d. Then, extrapolating these results, we determined the order of the PT under the suppressing rule in the thermodynamic limit.

We now briefly show numerical results and then theoretical results, of which derivations are presented in (*29*). First, for a given m, $G_m(t) = 0$ for $t < t_{cm}$. For $t_c < t < t_{cm}$, a spanning cluster is not created because of the suppressing rule, whereas it is formed in ordinary percolation. However, for $m > 1$ and $t > t_{cm}$, once one bridge bond is occupied, no further bonds are suppressed and thus the spanning cluster is not modified. Thus, $G_m(t)$ follows the curve of $G_1(t)$ for $t > t_{cm}$ (Fig. 2A). Therefore, there exists a finite discontinuity $G_1(t_{cm})$ at t_{cm}. In the reverse evolution, dynamics proceeds under the bias of sustaining the spanning cluster. For this case, evolution can be understood as the opposite procedure—that is, from occupation to deletion of bonds. Then, the spanning cluster can sustain up to $1 - t_{cm}$, but its size reduces to N_{BB}/N_b, where N_{BB} is the number of bridge bonds. In the thermodynamic limit, the fraction N_{BB}/N_b is zero in the interval $[1 - t_{cm}, 1 - t_c]$ for $d < 6$ (*20*). Thus, the order parameter behaves as shown in Fig. 2B.

Next, we plot the percolation threshold for systems with linear size L, $t_{cm}(L)$, versus L for several values of m. We find that $t_{cm}(L)$ decreases and converges to t_c as L increases for $m = 2$, and that $t_{cm}(L)$ increases and converges to 1 as L increases for $m \geq 3$ in two dimensions. More generally, we find that there exists a critical value $m_c(d) = d/(d - d_{BB})$ for $d > d_{BB}$, where d_{BB} is the fractal dimension of the set of bridge bonds (*20*), such that if $m < m_c$, $t_{cm}(L)$ decreases and converges to t_c as L increases, and if $m > m_c$, $t_{cm}(L)$ increases and converges to 1 as L increases. This is shown in Fig. 2C for two dimensions, and in fig. S2, A and C, for three and four dimensions, respectively. The analytic solution for $m_c(d)$ is presented in (*29*). It is estimated that $m_c(d) \approx 2.55 \pm 0.01$ ($d = 2$), 5.98 ± 0.07 ($d = 3$), 16.99 ± 5.23 ($d = 4$), 50 ($d = 5$), and ∞ ($d = 6$). For $d = 5$, the standard deviation is larger than the mean value. d_{BB} is equal to d in $d = 6$, which is thus the upper critical dimension, and the formula for m_c is valid for $d < d_c = 6$. To simulate for non-integer m cases, once we select an unoccupied bond randomly, and if that bond is a bridge bond, then it is occupied with the probability $q(t)^{1-(1/m)}$, where $q(t)$ is the probability that m potential bonds are all bridge bonds. Otherwise, it is always occupied. This dynamic process can be implemented without choosing m different unoccupied bonds, but by choosing just one bond.

Subsequently, we check the convergence rates for $t_{cm}(L) - t_c$ and $1 - t_{cm}(L)$ as a function of L. We obtain power-law behaviors, $t_{cm}(N) - t_c \sim N^{-1/\bar{\nu}_<}$ and $1 - t_{cm}(N) \sim N^{-1/\bar{\nu}_>}$, where the exponents $\bar{\nu}_<$ and $\bar{\nu}_>$ are derived analytically (*29*) as $1/\bar{\nu}_< = [1 - (m/m_c)]/(m\zeta + 1)$ and $1/\bar{\nu}_> = [(m/m_c) - 1]/(m - 1)$. The exponent $\bar{\nu}$ is rewritten as $d\nu$, where d is the spatial dimension and ν is the exponent characterizing the scaling relation between length scale L and the occupation probability t. These results are shown in Fig. 2, D and E, for two dimensions, and in fig. S2, B and D, for three and four dimensions, respectively. We show in (*29*) that the standard deviation for the statistical fluctuations of the critical point $t_{cm}(N)$ behaves in the same manner as $\sigma_< \sim N^{-1/\bar{\nu}_<}$ for $m < m_c$ and $\sigma_> \sim N^{-1/\bar{\nu}_>}$ for $m > m_c$, and this is confirmed

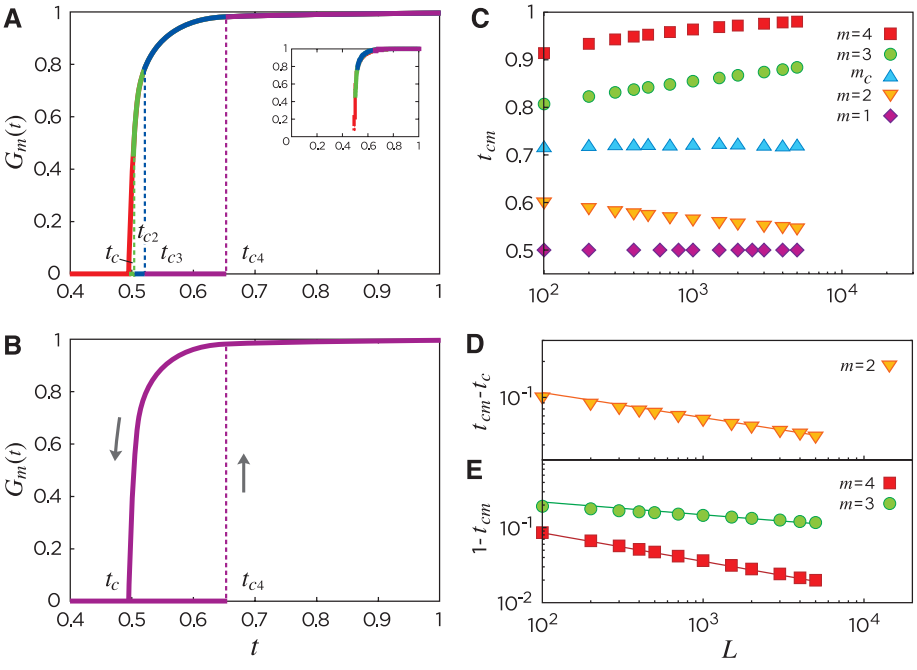

Fig. 2. (**A**) Schematic plot of the spanning cluster size $G_m(t)$ versus t, the number of attached bonds per N_b for the SCA model, with $m = 1$ (red), 2 (green), 3 (blue), and 4 (purple). Inset: Same plot with real data, which are obtained after averaging over the samples containing nonzero $G_m(t)$ at each time t. Data are obtained for a system size of $N = 10^6$ in two dimensions. (**B**) Hysteresis curve of the order parameter in forward and backward evolution. (**C**) Plot of $t_{cm}(L)$ versus L for various values of m. (**D**) Plot of $t_{cm}(L) - t_c$ for $m = 2$ versus L, which is the case $m < m_c$. (**E**) Plot of $1 - t_{cm}(L)$ for $m = 3$ and 4 versus L, which is the case $m > m_c$. Solid lines are guidelines with the slopes theoretically predicted. All data are averaged over 10^4 configurations.

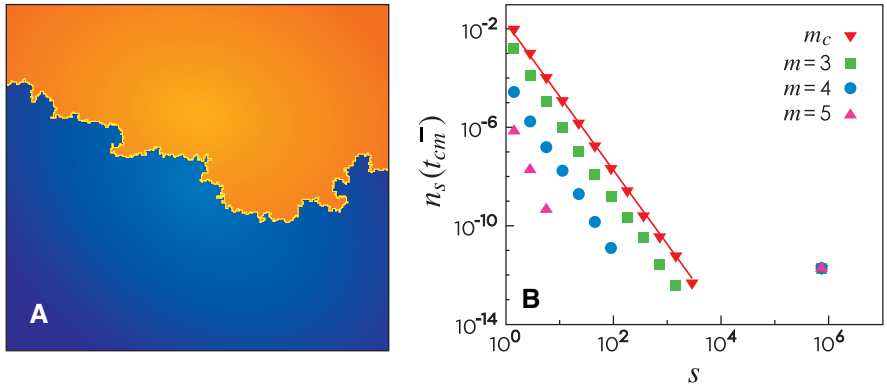

Fig. 3. (**A**) Plot of the giant and second largest clusters just before the percolation threshold $\bar{t}_{c4}$ for $m = 4$. Clusters are compact and the boundary is self-affine, with fractal dimension $d_{BB} \approx 1.22$. In general, for sufficiently large m, only very few clusters remain at $\bar{t}_{cm}(N)$. (**B**) Plot of n_s versus s at $\bar{t}_{cm}$ for $m = 3$, 4, 5, and $m_c \approx 2.55$ in two dimensions. Simulations are performed for $N = 10^6$, and the data are averaged over 10^3 configurations. The solid line is a guideline with slope −3.

numerically in fig. S1B. Note that at a tricritical point m_c, $t_{cm_c}(L \to \infty)$ is finite; for example, $t_{cm_c}(\infty) \approx 0.72$ in two dimensions, which is neither t_c nor unity, and the fluctuation is large and independent of N.

On the basis of the above results, we come to the conclusion that for $d < d_c = 6$, the percolation threshold in the limit $N \to \infty$ is t_c for $m < m_c$, finite t_{cm} at $m = m_c$, and 1 for $m > m_c$ [(*29*), equations 8 to 10]. For $d \geq d_c$, $m_c \to \infty$, and for finite m, $t_{cm} \to t_c$ (*29*). We conclude that when m is finite, the PT is continuous in the limit $N \to \infty$. In statistical physics, it is known that mean-field results above the upper critical dimension are equivalent to the solution on sparse random graphs. From this perspective, our result for $d > d_c$ is comparable to previous results for the EP model (*10*) on random graphs.

For the SCA model in the regime $m > m_c$ at $t_{cm}^{-}(L)$, we find that there are only a few clusters and that they are compact (Fig. 3A). Thus, the cluster size distribution at $t_{cm}^{-}(L)$ decays rapidly in the region of small cluster size and exhibits a peak in the region of large cluster size (Fig. 3B). The interface between clusters forms naturally along the bridge bonds and is self-affine. Because of the presence of already macroscopically grown but not yet spanning clusters, the order parameter is increased drastically when occupying a bridge bond. Finally, we note that for $d \geq d_c$, a discontinuous PT can take place if m varies with the system size N. We obtain a characteristic value $m_c \sim \ln N$ such that when m increases with N slower than m_c, the PT is continuous, and when m increases with N faster than m_c, the PT is discontinuous. They occur at t_c and 1, respectively [see (*29*)].

For the product rule (*4*), the nature of the PT is similar to the mean-field behavior of the SCA model in low dimensions such as $d = 2$. Under the best-of-m strategy, when m varies with the system size as $m > m_c \sim \ln N$, clusters are also compact and the number of clusters is limited to a finite value, and thus a discontinuous PT can take place. However, for a fixed m and in the thermodynamic limit, the PT is continuous [see (*29*)].

References and Notes

1. D. Stauffer, A. Aharony, *Introduction to Percolation Theory* (Taylor & Francis, London, ed. 2, 1994).
2. R. Pastor-Satorras, A. Vespignani, *Phys. Rev. Lett.* **86**, 3200 (2001).
3. M. Girvan, M. E. J. Newman, *Proc. Natl. Acad. Sci. U.S.A.* **99**, 7821 (2002).
4. D. Achlioptas, R. M. D'Souza, J. Spencer, *Science* **323**, 1453 (2009).
5. P. Erdös, A. Rényi, *Publ. Math. Inst. Hungar. Acad. Sci* **5**, 17 (1960).
6. R. M. Ziff, *Phys. Rev. Lett.* **103**, 045701 (2009).
7. Y. S. Cho, J. S. Kim, J. Park, B. Kahng, D. Kim, *Phys. Rev. Lett.* **103**, 135702 (2009).
8. F. Radicchi, S. Fortunato, *Phys. Rev. Lett.* **103**, 168701 (2009).
9. R. A. da Costa, S. N. Dorogovtsev, A. V. Goltsev, J. F. F. Mendes, *Phys. Rev. Lett.* **105**, 255701 (2010).
10. O. Riordan, L. Warnke, *Science* **333**, 322 (2011).
11. P. Grassberger, C. Christensen, G. Bizhani, S.-W. Son, M. Paczuski, *Phys. Rev. Lett.* **106**, 225701 (2011).
12. H. K. Lee, B. J. Kim, H. Park, *Phys. Rev. E* **84**, 020101(R) (2011).
13. N. Bastas, K. Kosmidis, P. Argyrakis, *Phys. Rev. E* **84**, 066112 (2011).
14. W. Choi, S.-H. Yook, Y. Kim, *Phys. Rev. E* **84**, 020102 (2011).
15. K. Panagiotou, R. Spöhel, A. Steger, H. Thomas, *Electron. Notes Discrete Math.* **38**, 699 (2011).
16. Y. S. Cho, B. Kahng, *Phys. Rev. Lett.* **107**, 275703 (2011).
17. W. Chen, R. M. D'Souza, *Phys. Rev. Lett.* **106**, 115701 (2011).
18. N. A. M. Araújo, H. J. Herrmann, *Phys. Rev. Lett.* **105**, 035701 (2010).
19. N. A. M. Araújo, J. S. Andrade Jr., R. M. Ziff, H. J. Herrmann, *Phys. Rev. Lett.* **106**, 095703 (2011).
20. K. J. Schrenk, N. A. M. Araújo, J. S. Andrade Jr., H. J. Herrmann, *Sci. Rep.* **2**, 348 (2012).
21. J. Nagler, A. Levina, M. Timme, *Nat. Phys.* **7**, 265 (2011).
22. H. D. Rozenfeld, L. K. Gallos, H. A. Makse, *Eur. Phys. J. B* **75**, 305 (2010).
23. J. Gómez-Gardeñes, S. Gómez, A. Arenas, Y. Moreno, *Phys. Rev. Lett.* **106**, 128701 (2011).
24. D. D. Martino, L. Dall'Asta, G. Bianconi, M. Marsili, *Phys. Rev. E* **79**, 015101(R) (2009).
25. R. K. Pan, M. Kivelä, J. Saramäki, K. Kaski, J. Kertész, *Phys. Rev. E* **83**, 046112 (2011).
26. Y. Azar, A. Z. Broder, A. R. Karlin, E. Upfal, *SIAM J. Comput.* **29**, 180 (1999).
27. M. Mitzenmacher, *IEEE Trans. Parallel Distrib. Syst.* **12**, 1094 (2001).
28. O. Riordan, L. Warnke, *Ann. Appl. Probab.* **22**, 1450 (2012).
29. See supplementary materials on *Science* Online.

Acknowledgments: We thank the referees for useful comments. Supported by National Research Foundation grant 2010-0015066 awarded through the Acceleration Research Program, the Seoul Science Foundation, and the Global Frontier Program (Y.S.C.).

Supplementary Materials

www.sciencemag.org/cgi/content/full/339/6124/1185/DC1
Supplementary Text
Figs. S1 to S11
Table S1

27 September 2012; accepted 28 January 2013
10.1126/science.1230813

Emergence of a Measurement Basis in Atom-Photon Scattering

Yinnon Glickman, Shlomi Kotler, Nitzan Akerman, Roee Ozeri*

After measurement, a wave-function is postulated to collapse on a predetermined set of states—the measurement basis. Using quantum process tomography, we show how a measurement basis emerges in the evolution of the electronic spin of a single trapped atomic ion after spontaneous photon scattering and detection. This basis is determined by the excitation laser polarization and the direction along which the photon was detected. Quantum tomography of the combined spin-photon state reveals that although photon scattering entangles all superpositions of the measurement-basis states with the scattered photon polarization, the measurement-basis states themselves remain classically correlated with it. Our findings shed light on the process of quantum measurement in atom-photon interactions.

The interaction between quantum systems and their environment results in decoherence and reduction of quantum superpositions to classical statistical ensembles. On the other hand, probing a fraction of the environment (environments by nature are too large to be monitored as a whole) yields information about the system state. The back-action on the system can then result in the emergence of a measurement basis. The measurement basis states will be those that are classically correlated with the detected environment modes, whereas their superpositions will be entangled with the environment (*1*, *2*). Thus, decoherence, measurement, and entanglement all partake in the quantum measurement process.

Because atomic systems can be well isolated from their environment and coherently controlled with good fidelity, they are a good experimental platform for the study of such fundamental quantum phenomena. In a typical experiment, a bipartite atomic superposition is controllably coupled to its environment and monitored in order to investigate different facets of decoherence and measurement. Examples include the study of decoherence due to coupling to engineered reservoirs by using trapped atomic ions (*3*) or the observation of the progressive decoherence of the measurement apparatus by using the interaction between atoms and a microwave cavity (*4*).

A natural environment for atomic systems is the electromagnetic vacuum to which they couple via spontaneous photon scattering. The effect of light scattering on the coherence of atomic interferometers showed that scattered photons expose the path an atom has taken (*5*–*7*). Photon scattering by trapped atomic ions, in which the direction and magnitude of the internal angular momentum of an atom become correlated with a scattered photon, results in spin decoherence (*8*–*10*). State-selective florescence by use of resonant laser light was used to measure the internal electronic state of atoms with a very small error probability (*11*–*13*). Last, the entanglement between a single atom and a spontaneously scattered photon was recently observed (*10*, *14*, *15*). In all of these experiments, decoherence, measurement, and entanglement

Department of Physics of Complex Systems, Weizmann Institute of Science, Rehovot 76100, Israel.

*To whom correspondence should be addressed. E-mail: roee.ozeri@weizmann.ac.il